The Astrophysical Journal, 950:16 (11pp), 2023 June 10 https://doi.org/10.3847/1538-4357/acce37

Does Feedback from Supermassive Black Holes Coevolve with the Host in Type 2 Quasars?

S. Jin[1], J. Wang[2,3], M. Z. Kong[1], R. J. Shen[4,5], Y. X. Zhang[6], D. W. Xu[3,7], J. Y. Wei[3,7], and Z. Xie[1]
[1] College of Physics, Hebei Normal University, Shijiazhuang 050024, People's Republic of China; kmz@hebtu.edu.cn
[2] Guangxi Key Laboratory for Relativistic Astrophysics, School of Physical Science and Technology, Guangxi University, Nanning 530004, People's Republic of China; wj@nao.cas.cn
[3] Key Laboratory of Space Astronomy and Technology, National Astronomical Observatories, Chinese Academy of Sciences, 20A Datun Road, Chaoyang District, Beijing 100101, People's Republic of China
[4] Purple Mountain Observatory and Key Laboratory of Radio Astronomy, Chinese Academy of Sciences, 10 Yuanhua Road, Nanjing 210033, People's Republic of China
[5] School of Astronomy and Space Science, University of Science and Technology of China, Hefei, Anhui 230026, People's Republic of China
[6] National Astronomical Observatories, Chinese Academy of Sciences, 20A Datun Road, Chaoyang District, Beijing 100101, People's Republic of China
[7] School of Astronomy and Space Science, University of Chinese Academy of Sciences, Beijing, People's Republic of China
Received 2023 January 11; revised 2023 April 13; accepted 2023 April 15; published 2023 June 7

Abstract

The feedback from the accretion of central supermassive black holes (SMBHs) is a hot topic in the coevolution of SMBHs and their host galaxies. By tracing the large-scale outflow using the line profile and bulk velocity shift of [O III]λ5007, the evolutionary role of outflow is studied here on a large sample of 221 type 2 quasars (QSO2s) extracted from Reyes et al. By following our previous study on local Seyfert 2 galaxies, the current spectral analysis on the Sloan Digital Sky Survey spectroscopic database enables us to arrive at the following results: (1) by using the Lick indices, we confirm that QSO2s are, on average, more frequently associated with younger stellar populations than Seyfert galaxies; (2) QSO2s with a stronger outflow tend to be associated with a younger stellar population, which implies a coevolution between the feedback from SMBHs and the host in QSO2s; (3) although occupied at the high $L_{\rm bol}/L_{\rm Edd}$ end, the QSO2s follow the $L_{\rm bol}/L_{\rm Edd}$-$D_n(4000)$ sequence established from local, less-luminous Seyfert galaxies, which suggests a decrease of the accretion activity of SMBHs and also of feedback as the circumnuclear stellar population continuously ages.

Unified Astronomy Thesaurus concepts: Galaxy evolution (594); Quasars (1319); Active galactic nuclei (16)

1. Introduction

There is accumulating evidence supporting the fact that the feedback process from supermassive black holes (SMBHs) plays an important role in the conception of the coevolution of growth of SMBHs and their host galaxies where the SMBHs reside (see reviews in Heckman et al. 2004; Alexander & Hickox 2012; Fabian 2012). In both secular and merger evolutionary scenarios proposed in past decades (e.g., Sanders et al. 1988; Di Matteo et al. 2008; Hopkins et al. 2008b; Hopkins & Hernquist 2009; Hopkins et al. 2013; Draper & Ballantyne 2012; Shankar et al. 2012; Heckman & Best 2014), feedback is generally required in not only semianalytic models but also in numerical simulations to self-regulate the growth of SMBHs and star formation that occurs in the host galaxy by either suppressing star formation by sweeping out circumnuclear gas or triggering star formation by compressing the gas (e.g., Alexander & Hickox 2012; Page et al. 2012; Kormendy & Ho 2013; Zubovas et al. 2013; Ishibashi & Fabian 2014; Cresci et al. 2015; Carniani et al. 2016; Villar et al. 2016; Woo et al. 2017; Cresci & Maiolino 2018; Perna et al. 2020; Scholtz et al. 2021; Shin et al. 2021).

In fact, the models with feedback can reproduce the firmly established $M_{\rm BH}$–$\sigma_\star$ relation and luminosity functions of both quasars and normal galaxies (e.g., Haehnelt et al. 1998; Silk & Rees 1998; Fabian 1999; Kauffmann & Haehnelt 2000; Granato et al. 2004; Springel et al. 2005; Croton et al. 2006; Di Matteo et al. 2007; Hopkins et al. 2008b; Khalatyan et al. 2008; Menci et al. 2008; Somerville et al. 2008). Furthermore, the "overcooling" problem in the Lambda cold dark matter (ΛCDM) galaxy formation model can be solved by additional heating contributed by the feedback from SMBHs (e.g., Ciotti & Ostriker 2007; Somerville et al. 2008; Hirschmann et al. 2014).

On the observational ground, the feedback is usually traced by the frequently observed outflows from central SMBHs in order to study not only its origin but also its effect on host galaxies (see reviews in Veilleux & Rupke 2005; Fabian 2012). Among the different diagnoses of the outflows, the most used is the blue asymmetry of the prominent [O III]$\lambda\lambda$4959,5007 doublet and its bulk blueshift with respect to the local system, which is found to be quite prevalent in both local and distant active galactic nuclei (AGNs; e.g., Heckman et al. 1981; Véron-Cetty et al. 2001; Zamanov et al. 2002; Marziani et al. 2003; Aoki et al. 2005; Boroson 2005; Komossa et al. 2008; Xu & Komossa 2009; Villar-Martín et al. 2011; Liu et al. 2013; Mullaney et al. 2013; Zhang et al. 2013; Harrison et al. 2014; Villar Martín et al. 2014; Karouzos et al. 2016; Wang et al. 2016, 2018).

Using the line profile of the [O III] line emission, Wang et al. (2011) performed a comprehensive study on a large sample of local, obscured AGNs, which were extracted from the MPA-JHU value-added catalog (e.g., Kauffmann et al. 2003) and based on the Sloan Digital Sky Survey (SDSS; e.g., York et al. 2000), to explore the relation between outflows and properties of the host galaxies according to the widely accepted AGN

unification model (e.g., Antonucci 1993), in which the central AGN's continuum and emissions from the broad-line region (BLR) are obscured by the torus. The authors proposed a trend that the local Seyfert 2 galaxies with stronger blue asymmetries tend to be associated with not only younger stellar populations but also a higher AGN Eddington ratio ($L/L_{\rm Edd}$, where $L_{\rm Edd} = 1.26 \times 10^{38} M_{\rm BH}/M_{\odot}$ erg s^{-1} is the Eddington luminosity). This result is further confirmed in Wang (2015) for a sample of nearby partially obscured AGNs.

A question therefore naturally arises: is the dependence of the strength of outflow on both stellar population ages and $L/L_{\rm Edd}$ revealed in local Seyfert galaxies still valid for either their high-luminosity or high-redshift cousin? This question is motivated by two facts. On the one hand, there is ample evidence supporting the idea that the growth of small SMBHs in low-luminosity AGNs (e.g., Seyfert galaxies) is dominantly through a secular evolution in which the gas inflow toward a central SMBH is mainly caused by an instability or viscousness of the gas (e.g., Heckman & Best 2014; Wang et al. 2016, 2019, and references therein). In contrast, a gas-rich major merger is preferred for the luminous quasars with a large SMBH, as implied by the studies of the host galaxies of quasars and ultra-luminous infrared galaxies (e.g., Sander & Friedl 1988; Bahcall et al. 1997; Kirhakos et al. 1999; Hao et al. 2005; Hou et al. 2011). On the other hand, the cosmic coevolution of SMBH growth and star formation implies that the feedback from AGNs is strong in the early universe when the peaks of both AGN activity and star formation occur roughly coincident (e.g., Hou et al. 2011; Ishibashi et al. 2013; Harrison 2017).

In this paper, we try to answer the aforementioned question by extending the study in Wang et al. (2011) to type 2 quasars (QSO2s), the high-luminosity counterparts of the local Seyfert 2 galaxies. In fact, previous studies through different methods indicate that the outflow phenomenon is quite popular in QSO2s (e.g., Villar-Martín et al. 2011; Villar Martín et al. 2014; Liu et al. 2013; Karouzos et al. 2016; Ramos Almeida et al. 2017). The scale of the violent outflow in quasi-stellar objects (QSOs) ranges from a few parsecs ($v \sim 0.1c$) to $\sim$1 kpc ($v \sim 10^{2-3}$ km s^{-1}) (e.g., Pounds et al. 2003; Harrison et al. 2016; Förster Schreiber et al. 2019; Kakkad et al. 2020). An outflow with an extension of 13 pc from the center of an SMBH has been identified for the ionized gas in the obscured AGN XID 2028 at $z = 1.59$ (Carniani et al. 2016), which is recently confirmed by the Early Release Science JWST NIRSpec observations (e.g., Cresci et al. 2023). Compared with the Very Large Array 3 GHz map, the authors argue that the extended outflow in the object is likely related to the low-luminosity radio jet.

The outline of this paper is as follows. The sample selection and spectral analysis are described in Sections 2 and 3, respectively. Section 4 shows the statistical results. A discussion is presented in Section 5. A ΛCDM cosmology with parameters $H_0 = 70$km s^{-1} Mpc^{-1}, $\Omega_m = 0.3$, and $\Omega_\Lambda = 0.7$ (Spergel et al. 2003) is used throughout the paper.

2. Sample Selection

A couple of QSO2s samples have been published in past decades (e.g., Zakamska et al. 2003; Reyes et al. 2008; Yuan et al. 2016) thanks to the SDSS. We start from the QSO2s sample provided by Reyes et al. (2008), simply because Kong & Ho (2018) performed a comprehensive study on their black hole mass and $L_{\rm bol}/L_{\rm Edd}$ by adopting the narrow emission lines, such as [O III]λ5007 as an indicator. The used QSO2s catalog contains a total of 887 objects with redshift $z < 0.83$, whose [O III]λ5007 line luminosity ranges from $10^{8.3}$ to $10^{10.0} L_{\odot}$. They are selected from the seventh data release of SDSS (Abazajian et al. 2009) by following the four main selection rules (please see selection details in Zakamska et al. 2003; Reyes et al. 2008):

1. In order to retain objects with a weak continuum and strong narrow [O III]λ5007 emission lines, the rest-frame equivalent width is greater than 4 Å and the corresponding signal-to-noise ratio (S/N) is $\geqslant$7.5 over the entire spectroscopic range of 3800–9200 Å.
2. For objects with $z < 0.36$, Hβ+[O III] $\lambda\lambda$4959,5007, Hα +[N II] $\lambda\lambda$6548,6583, and [S II]$\lambda\lambda$6716,6731 lines are required to be available. AGNs are distinguished from star-forming galaxies using the line ratio diagnostic criteria presented by Kewley et al. (2001), i.e., $\log([\mathrm{O\,III}]/\mathrm{H}\beta) > \frac{0.61}{\log([\mathrm{N\,II}]6583\,/\,\mathrm{H}\alpha) - 0.47} + 1.19$, and $\log([\mathrm{O\,III}]/\mathrm{H}\beta) > \frac{0.72}{\log([\mathrm{S\,II}]\,/\,\mathrm{H}\alpha) - 0.32} + 1.30$.
3. For objects with redshift $0.36 \leqslant z < 0.83$, the Hβ line is required to either be undetected or have a line ratio of $\log \frac{[\mathrm{O\,III}]\,5007}{\mathrm{H}\beta} > 0.3$ if the flux of the Hβ line is available with S/N > 3.
4. Moreover, for objects with $z > 0.6$, the FWHM of the Mg IIλ2800 emission line is required to be less than 2000 km s^{-1} if the line is above the noise level.

The SDSS spectra of the 887 QSO2s candidates were then checked visually by us one by one. More than 40 objects with unambiguous double-peaked line profiles were excluded to avoid unreliable [O III] λ5007 emission-line profile measurements. The double-peaked profiles may be caused by galaxy mergers, disk rotation on a large scale, or bipolar outflows (e.g., Liu et al. 2010; Ge et al. 2012). Objects with either a [O III] line S/N less than 10 or an incomplete line profile were additionally removed. As a result, there are 772 QSO2s for subsequent spectral analysis.

3. Spectral Analysis

For each of the objects listed in the sample, the SDSS spectrum is at first corrected for Galactic extinction by using the extinction curve of Cardelli et al. (1989) and the extinction value adopted from Schlafly & Finkbeiner (2011). The redshift provided by the SDSS pipelines is then used to transform the observed spectrum to the rest frame.

3.1. Continuum and Stellar Subtraction

Before the [O III] emission-line measurements, the underlying stellar component including stellar continuum and stellar absorption features must be carefully subtracted. This subtraction was carried out using the publicly automatic procedure of the penalized pixel-fitting (pPXF) method (Cappellari & Emsellem 2004; Cappellari 2017). We refer the readers to Kong & Ho (2018) for the details of the stellar component subtraction for this sample and stress here some key issues as follows:

1. The spectral fitting region covers 4100–5400 Å, including Hβ, [O III] λ5007 emission line.

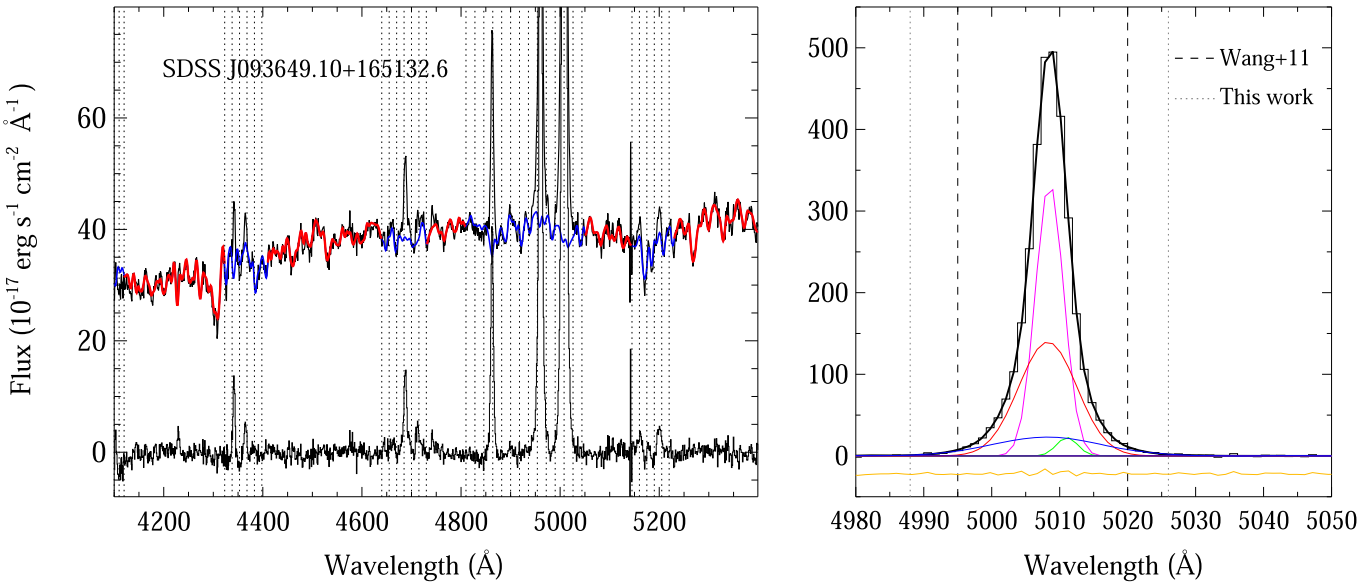

Figure 1. Left: an example of continuum/stellar subtraction. The original and continuum-removed spectra are displayed by the upper and lower black curves, respectively. The best-fitted stellar component is overplotted with the red and blue colors for the fitting region and the region excluded in the fitting, respectively. Right: the [O III]λ5007 line profile modeled by a linear combination set of Gaussian components after the removal of the continuum. The observed and modeled line profiles are plotted with thin and heavy black solid lines, respectively. Each Gaussian component is plotted with a thin colorful line. The orange curve below the line spectrum presents the residuals between the observed and modeled emission-line profiles. The vertical long and short dashed lines mark the wavelength regions used for measuring the line profile parameters in Wang et al. (2011) and in this work, respectively.

2. The Indo-U.S. stellar spectral library (Valdes et al. 2004) is adopted for fitting the continuum of the host galaxies. The stellar spectral library has a spectral resolution of FWHM = 1.35 Å and a wavelength range of 3460–9464 Å.
3. The IDL package `mpfit` (Markwardt 2009) is used to determine the best-fitted parameters through a χ^2 minimization in which the nonlinear Levenberg–Marquardt algorithm is adopted.
4. In addition to the strong emission lines (such as He II λ4686, Hβ, and [O III]$\lambda\lambda$4959,5007), the Hγ λ4340, [O III] λ4363, [O II]λ3727, [Ne III]λ3869, and Mg I*b* $\lambda\lambda$5167,5173,5184 triplets are excluded from the fitting. The Mg I*b* triplets were also masked because of their potential systematic effects caused by [Mg/Fe] enhancement.

An example of continuum and stellar fitting can be seen in the left panel in Figure 1.

3.2. Measurements of Emission-line Profile Parameters

After the continuum and absorption stellar components are subtracted from each spectrum, a set of shape parameters are measured for the [O III] line profile in this section.[8]

3.2.1. Line Profile Fitting

Many ways are used to parameterize an emission-line profile. Parameters including the FWHM and the second moment of the line are commonly used. The second moment is defined to be

$$\sigma^2 = \left(\frac{c}{\lambda_c}\right)^2 \frac{\int (\lambda - \lambda_c)^2 f_\lambda \, d\lambda}{\int f_\lambda \, d\lambda}, \quad (1)$$

where f_λ is the flux density of the continuum-subtracted spectrum and λ_c is the line centroid and is defined as $\overline{\lambda} = \int \lambda f_\lambda \, d\lambda / \int f_\lambda \, d\lambda$. Both parameters comparably describe the line broadening for a pure Gaussian profile, i.e., FWHM $= 2\sqrt{2\ln 2}\,\sigma \approx 2.35\sigma$. As described in Greene & Ho (2005), σ is more sensitive to the line wings and becomes relatively broader, which indicates that σ contains more information on the line profile broadening if the profile is not a pure Gaussian profile. In fact, in addition to σ, as presented in Binney & Merrifield (1998), ξ_3 and ξ_4, which are the high-order dimensionless line shape parameters, can be used to parameterize line profile deviation from a pure Gaussian profile.

ξ_k is defined as

$$\xi_k = \mu_k / \sigma^k \; k \geqslant 3, \quad (2)$$

where σ is the second moment defined above, and μ_k the k-order moment defined below

$$\mu_k = \left(\frac{c}{\overline{\lambda}}\right)^k \int (\lambda - \overline{\lambda})^k f_\lambda \, d\lambda. \quad (3)$$

ξ_3, the so-called "skewness," measures a deviation from a symmetric profile. $\xi_3 = 0$ corresponds to a symmetry profile. Meanwhile, $\xi_3 > 0$ denotes a red asymmetry, and $\xi_3 < 0$ a blue asymmetry.

ξ_4, the so-called "kurtosis," measures a symmetric deviation from a pure Gaussian profile with $\xi_4 = 3$. $\xi_4 > 3$ corresponds to a peaked emission-line profile superposed on a broad base, and $\xi_4 < 3$ to an emission-line profile in a "boxy" shape. We refer the readers to Figure 11.5 in Binney & Merrifield (1998) for

[8] As illustrated in Figure 1, the continuum removal is necessary before an emission-line analysis in type II AGNs, because the measured [O III] line profile asymmetry strongly depends on the behavior of the line wing and the determined continuum level, which can be distorted heavily by the absorption features of the starlight component.

how, in detail, the line shapes change with the values of ξ_3 and ξ_4.

The [O III]λ5007 blue wings are found to overlap with the [O III] λ4959 lines in some objects with strong outflows. In order to avoid a distortion due to this overlapping, we first fit each [O III] doublet with a linear combination of a set of Gaussian components, in which the doublets have the same width and fixed line flux ratio of the theoretical value of 1:3. An example of the profile modeling is shown in the right panel of Figure 1.

The [O III]λ5007 line profile parameters are then measured from the modeled line profile. The wavelength range over which the line profile parameters are measured should be carefully chosen. A wavelength range of 4995–5020 ÅÅ was used for measuring ξ_3 and ξ_4 in the Seyfert 2 galaxies sample in Wang et al. (2011). However, this wavelength range cannot cover most of the [O III] profiles well for the type 2 quasar sample, because their [O III] line profiles usually have relatively broader line wings. We therefore instead measure their parameters within the wavelength range where the line flux level is 2 times the continuum fluctuation that is assessed in the wavelength range free of strong emission or absorption lines, i.e., between 4400 and 4600 ÅÅ. In Section 3.2.5, we discuss the wavelength range effect on the parameter measurements.

3.2.2. Instrumental Resolution

The observed σ results from a convolution of the true line profile and the instrumental profile. By assuming the profiles can be described as a pure Gaussian function, the intrinsic line width σ can be estimated approximately by $\sigma^2 = \sigma^2_{\rm obs} - \sigma^2_{\rm inst}$, where $\sigma_{\rm obs}$ and $\sigma_{\rm inst}$ are the observed line width and the instrumental resolution, respectively. However, as stated in the Appendix of Wang et al. (2011), the correction of the instrumental resolution is not an easy task for a non-Gaussian line profile, where the correction depends on the amount of deviation from a pure Gaussian profile. In their work, only the [O III] line widths greater than $2\sigma_{\rm inst}$ were kept for subsequent analysis. By following this sample selection rule, there are only six objects with $\sigma_{\rm obs} < 2\sigma_{\rm inst}$, and 767 objects are left.

3.2.3. [O III]λ5007 Line Relative Velocity Shifts

Given the measured line centroids, $\overline{\lambda}$, we measure the bulk velocity shift of the [O III] emission line $\Delta\upsilon = \delta\lambda/\lambda_0 c$ in each stellar-subtracted emission-line spectrum, where $\delta\lambda$ is the [O III] line wavelength shift relative to the galaxy rest frame determined from the absorption features of the host galaxy, λ_0 is the wavelength of the [O III] emission line in the rest frame, and c is the light velocity. A positive value of $\Delta\upsilon$ denotes a red bulk velocity shift, and a negative one a blueshift.

3.2.4. $D_n(4000)$ and $H\delta_A$

The two Lick indices of $D_n(4000)$ (the 4000 Å break) and $H\delta_A$ (the equivalent width of the $H\delta_A$ absorption feature of A-type stars) are good age indicators of the stellar populations of galaxies (e.g., Bruzual 1983; Worthey & Ottaviani 1997; Balogh et al. 1999). The 4000 Å break is defined as $D_n(4000) = \int_{4000}^{4100} f_\lambda d\lambda \Big/ \int_{3850}^{3950} f_\lambda d\lambda$. The index $H\delta_A$ is defined as $H\delta_A = (4122.25\text{–}4083.50)(1 - F_I/F_C)$, where F_I is the flux within the feature bandpass of $\lambda\lambda$4083.50–4122.25, and F_C is the flux of the pseudocontinuum assessed from the two beside regions: blue $\lambda\lambda$4041.60–4079.75 and red $\lambda\lambda$4128.50–4161.00. In order to avoid distortion from unreliable values, the $D_n(4000)$ is measured for only 221 objects with not only a continuum median S/N >5 but also obvious stellar features, such as absorption lines of Ca II H,K $\lambda\lambda$ 3934,3968, after a one-by-one visual inspection. For each of the 221 objects, we measure both $D_n(4000)$ and $H\delta_A$ from the modeled starlight component, rather than the original spectrum, which suggests that the contamination caused by the [Ne III]λ3869 emission line is negligible for the resulting $D_n(4000)$. In addition, the adopted continuum S/N requirement leads to a bias against QSO2s at a high redshift. The redshifts of the 221 objects with measured $D_n(4000)$ actually range from 0.05 to 0.35, which shows overlaps with a fraction of the Seyfert galaxies with high redshifts (see Section 5.1 for the details). The distributions of the [O III]λ5007 line luminosity of the 221 QSO2s are shown and compared with those of the total sample in two redshift bins in Figure 2.

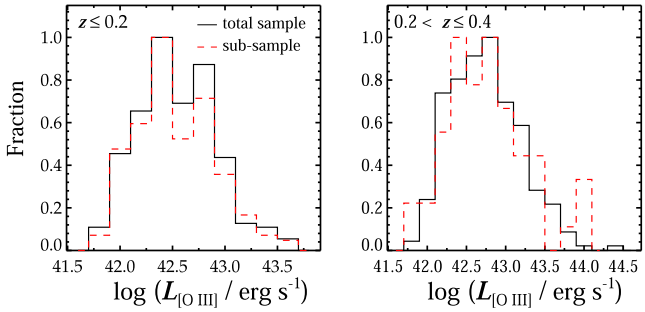

Figure 2. A comparison of the distributions of line luminosity of [O III]λ5007 in two redshift bins between the 221 QSOs used for subsequent statistic study and the parent QSO2s sample given in Reyes et al. (2008).

3.2.5. Wavelength Range Effect on ξ_3 and ξ_4

Before the subsequent statistical study, we first study the systematic of ξ_3 and ξ_4 due to different wavelength ranges where the two parameters are assessed. Based on the continuum flux fluctuation, estimated between 4400 and 4600 Å, both parameters are measured in three different wavelength ranges in which the specific line flux is above a base at different significance levels, $S/N_{\rm Min} = 1, 2, 3$, where $S/N_{\rm Min}$ is defined as the ratio between the level of the base and the continuum flux fluctuation.

We argue that the systematics on ξ_3, due to the adopted wavelength range, is negligible, although this is not true for ξ_4. Figure 3 compares the distributions of ξ_3 and ξ_4 measured within different wavelength ranges (or $S/N_{\rm Min}$). The corresponding median values are compared in Column (2) in Table 1. Columns (3)–(4) tabulate the matrix of two-sided Kolmogorov–Smirnov (K-S) tests, in which each entry denotes the maximum distance between the two distributions, along with the corresponding probability that the two distributions come from the same parent sample shown in the bracket. The tests show that there is no significant difference between the three distributions, although the larger the wavelength range used, the slightly higher the median of ξ_3 will be. However, with the increasing wavelength range, the distributions of ξ_4 clearly become wide, along with an increasing median value. The same tests yield a probability that the distributions are from the same parent sample, as low as $<10^{-6}$.

As an additional test, we measure both ξ_3 and ξ_4 by extending the wavelength range to 4000 km s^{-1} (about 60 Å),

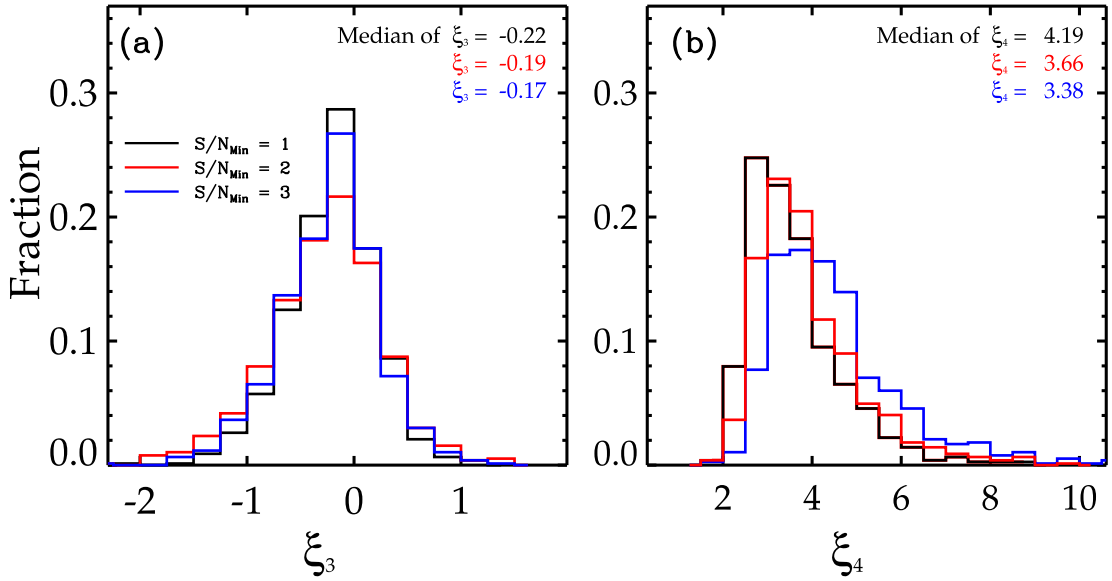

Figure 3. Distributions of ξ_3 (left panel) and ξ_4 (right panel) when they were measured at different wavelength ranges (or S/N_{Min}, see main text for the definition of S/N_{Min}).

Table 1
Median and Two-sided Kolmogorov–Smirnov Test Matrix of the [O III] Line Shape Parameters ξ_3 and ξ_4 Measured within the Different Wavelength Ranges

S/N_{Min} (1)	Median (2)	1 (3)	2 (4)	3 (5)
		ξ_3		
1	-0.22 ± 0.02	...	...	...
2	-0.19 ± 0.02	0.051 (0.267)	...	...
3	-0.17 ± 0.01	0.092 (0.003)	0.052 (0.241)	...
		ξ_4		
1	4.19 ± 0.05	...	...	...
2	3.66 ± 0.04	0.21 ($<10^{-15}$)	...	...
3	3.38 ± 0.03	0.32 ($<10^{-35}$)	0.14 ($<10^{-7}$)	...

which is twice the critical value that distinguishes the broad and narrow emission lines of AGNs. By comparing the values obtained with $S/N_{Min} = 1$, the change of the median ξ_3 is less than 1%, but the median of ξ_4 changes from 4.19 to 5.08. This test again verifies the above statement that the adopted wavelength range has a small (large) effect on measurements of ξ_3 (ξ_4).

Finally, without further statement, the values of both ξ_3 and ξ_4 measured under the condition of $S/N_{Min} = 2$ are adopted for subsequent statistical studies, taking into account a comparison with our previous studies in Wang et al. (2011) that was based on the observed spectra rather than the modeled line spectral profile.

4. Results

The measured parameters of the QSO2s are compared with our previous studies on Seyfert 2 galaxies in this section.

4.1. Statistic of Line Shape Parameters ξ_3 and ξ_4

The occupations in the ξ_3 versus ξ_4 diagram are compared between QSO2s and Seyfert 2 galaxies in Figure 4.

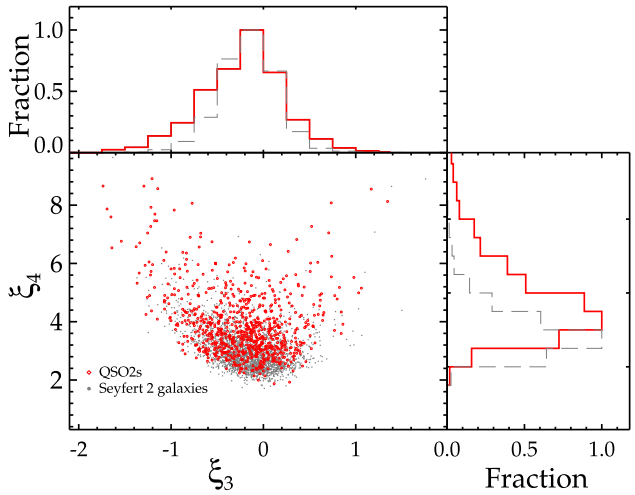

Figure 4. Main panel: a comparison between the QSO2s (red points) studied here and Seyfert 2 galaxies (gray points) quoted in Wang et al. (2011) in the ξ_3 vs. ξ_4 diagram. Upper left panel: distributions of the parameter ξ_3 for the QSO2s (red line) and Seyfert 2 galaxies (gray line). Bottom right panel: the same as the upper left panel, but for the parameter ξ_4. There are, in total, 767 objects with $\sigma_{obs} > 2\sigma_{inst}$ used in the plot.

The main panel in the figure shows that both QSO2s and Seyfert 2 galaxies form a sequence starting from the pure Gaussian region (i.e., $\xi_3 = 0$ and $\xi_4 = 3$) to the upper left corner. The larger the blue asymmetry of the [O III] line profile, the more a peaked profile will be identified, which is consistent with the fact that two or more Gaussian components are usually required to properly reproduce both the narrow core and blue wing of the observed [O III] line profiles.

The distributions of ξ_3 and ξ_4 are presented in the upper and right subpanels in Figure 4, respectively. Compared to the Seyfert 2 galaxies, the QSO2s tend to have stronger [O III] blue asymmetry. The median value of ξ_3 is -0.19 ± 0.02 for the QSO2s, and -0.16 ± 0.01 for the Seyfert 2 galaxies. A two-sided K-S test yields a difference between the two distributions at a significance level of $<10^{-14}$, with a maximum absolute discrepancy of 0.16. A significant difference can be found for

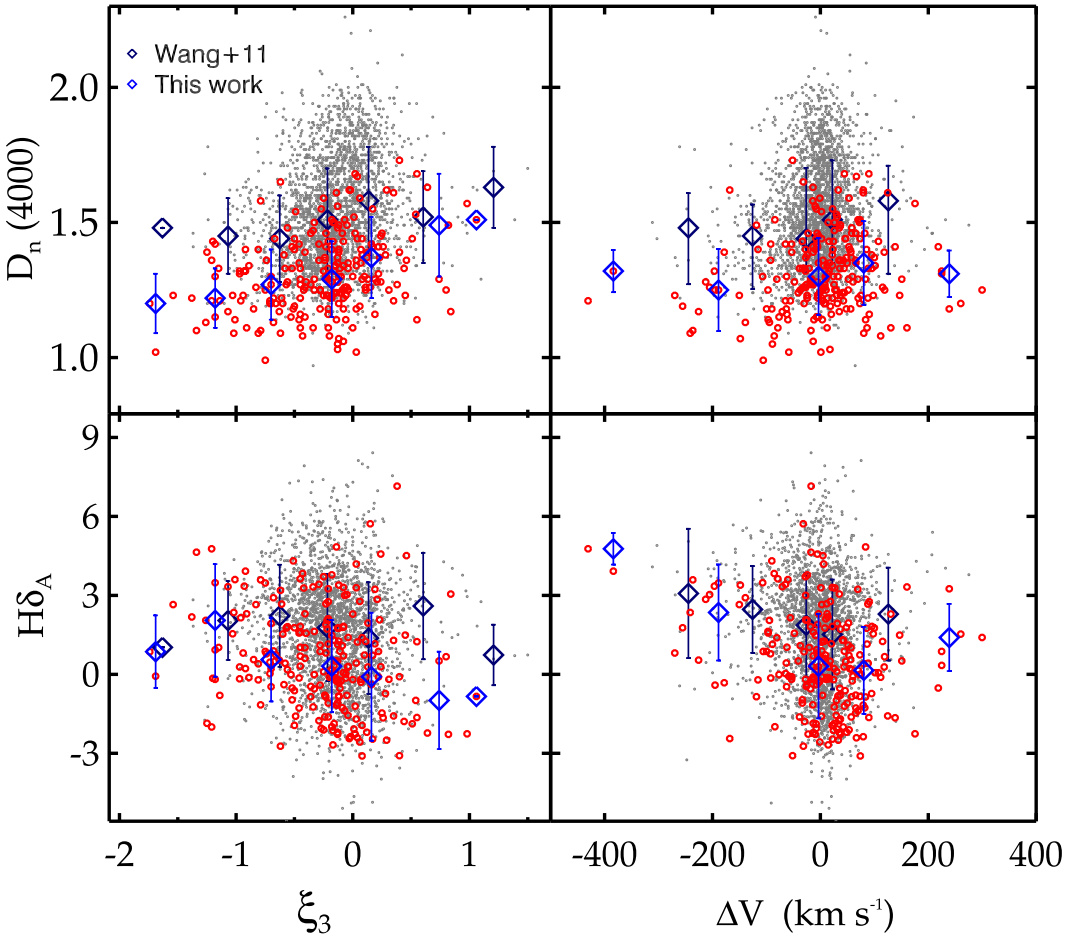

Figure 5. The Lick indices of $D_n(4000)$ and $H\delta_A$ plotted against the [O III] line shape parameters ξ_3 (left panels) and the relative bulk velocity shift ΔV (right panels). The QSO2s and Seyfert 2 galaxies are denoted by the red and gray dots, respectively. In each panel, the median $D_n(4000)$ and $H\delta_A$ values in each bin ($\Delta\xi_3 = 0.5$ and $\Delta V = 100$ km s^{-1}), along with the uncertainties, are overplotted by the diamonds (dark blue for the Seyfert galaxies and blue for the QSO2s).

the ξ_4 distributions, in which the median value of ξ_4 is 3.66 ± 0.04 for the QSO2s, and 2.84 ± 0.01 for the Seyfert 2 galaxies. Again, the same K-S test yields a difference at a significance level of $<10^{-6}$, with a maximum absolute discrepancy of 0.39. In fact, this significant discrepancy is not hard to understand as a result of the fact that QSO2s typically have stronger [O III] emissions (mostly contributed by the narrow line core) than local Seyfert 2 galaxies. The large ξ_4 also indicates that QSO2s have stronger [O III] wings than the Seyfert 2 galaxies.

4.2. Dependence of Line Profile on Stellar Population

The evolution of the [O III] line profile is examined in this section by using the two Lick indices $D_n(4000)$ and $H\delta_A$, which are widely used as age indicators of the circumnuclear stellar populations.

Both Lick indices are plotted against the ξ_3 and [O III]λ5007 line relative velocity shifts $\Delta\upsilon$ in Figure 5 for both QSO2s and Seyfert 2 galaxies.[9] One can see from the figure that, compared to the Seyfert 2 galaxies, the QSO2s are biased toward the small $D_n(4000)$ end. For the QSO2s sample, about 90% of the $D_n(4000)$ is less than 1.5, and there is almost no $D_n(4000)$ above 1.8. However, a large range extending to 2.0 can be found for the $D_n(4000)$ of the Seyfert 2 galaxies. The fact that $D_n(4000)$ increases with stellar population age therefore suggests a young stellar population in QSO2s. In fact, $D_n(4000) = 1.5$ is usually used to distinguish young stellar populations from old ones (Kauffmann et al. 2003). Based on Spearman's rank-order test, the corresponding correlation coefficients are tabulated in Table 2. For each entry, the value in the bracket is the probability that the two variables are not correlated. In addition to $D_n(4000)$, as shown in the figure, the bias against old stellar populations in QSO2s can also be learned from the lower two panels in which the $H\delta_A$ index is used.

To examine the dependence of the [O III] line profile on the stellar population, we divide the QSO2s into two groups, according to their ξ_3 values: one group has $\xi_3 > -0.5$ and the other has $\xi_3 < -0.5$, by following the method used in Wang et al. (2011). The corresponding distributions of $D_n(4000)$ and $H\delta_A$ are compared between the two groups in the two upper panels in Figure 6, respectively. These plots show that, similarly to in the Seyfert 2 galaxies, the QSO2s with relatively stronger blue asymmetry of the [O III] line profile tend to be associated with younger stellar populations, assessed by the smaller $D_n(4000)$ and larger $H\delta_A$. A similar result can be learned for $\Delta\upsilon$ from the two lower panels, in which the QSO2s with larger bulk blue velocity shifts tend to have younger stellar populations. The difference between the two distributions

[9] It is noted that the values of $\delta\upsilon$ in Wang et al. (2011) are calculated according to the narrow Hβ line for the Seyfert galaxies.

Table 2
Spearman Rank-order Correlation Coefficient Matrix

Property	$D_n(4000)$ (1)	$L_{\rm bol}/L_{\rm Edd}$ (2)
	Sample: QSO2s	
ξ_3	$0.31(1.9\times10^{-6})$	$-0.11(0.10)$
ξ_4	$-0.09(0.17)$	$0.35(8.6\times10^{-8})$
	Sample: QSO2s+Seyfert 2s	
ξ_3	$0.25(6.5\times10^{-24})$	$-0.21(2.4\times10^{-17})$
ξ_4	$-0.43(0)$	$0.50(0)$

shown in each panel of Figure 6 is examined by the two-sided K-S tests. The calculated maximum distance between the two distributions (see Figure 6 for the details) is tabulated in Table 3. The values in the brackets are the corresponding significance levels at which the two distributions come from the same parent sample.

4.3. Role of the Eddington Ratio

The Eddington ratio $L/L_{\rm Edd}$ is an important physical parameter driving the AGN's activity. Nelson et al. (2004) showed a correlation between the [O III]λ5007 line blue asymmetry and Eigenvector 1 space in the PG quasars. Shen & Ho (2014) confirmed that $L_{\rm bol}/L_{\rm Edd}$ is the main physical driver of the Eigenvector 1 space of the AGNs. Wang et al. (2011) indicated that stronger blue asymmetry is not only correlated with younger stellar populations but also with higher $L_{\rm bol}/L_{\rm Edd}$ for a sample of nearby Seyfert 2 galaxies. This trend was then confirmed by a sample of nearby partially obscured AGNs.

4.3.1. Estimation of L/L_{Edd}

In order to estimate $L_{\rm bol}/L_{\rm Edd}$ of the QSO2s, the bolometric luminosity $L_{\rm bol}$ is transformed from the intrinsic extinction-corrected [O III]λ5007 line luminosity $L_{[\rm O\ III]}$ through the bolometric correction $L_{\rm bol}/L_{[\rm O\ III]}\approx3500$ (Heckman et al. 2004), which is consistent with that used in Wang et al. (2011). The extinction-corrected $L_{[\rm O\ III]}$ is obtained from Kong & Ho (2018), in which the extinction was estimated from the observed Balmer decrement in the standard case B recombination (Halpern & Steiner 1983) and the extinction cure of Cardelli et al. (1989) with $R_V=3.1$. A median value of $\rm H_\alpha/H_\beta=4.04$ is adopted for the objects without a measured Balmer decrement.

The black hole mass $M_{\rm BH}$ of each object is estimated from the well-documented $M_{\rm BH}$–σ_* relationship: $\log(M_{\rm BH}/M_\odot)=8.13+4.02\log(\sigma_*/200\ {\rm km\ s^{-1}})$ (Tremaine et al. 2002), in which the stellar velocity dispersion of the bulge is replaced by the width of the core of the [O III] λ5007 line. As presented in Kong & Ho (2018), the width of the core of the [O III] line can trace the stellar velocity dispersion well for QSO2s. In addition, a heavy blend between the stellar absorption features and the AGN's emission lines, such as an overlap of Ca II H,K [N III] λ3968 and Hϵ lines, leads to a large uncertainty of the measured σ_*.

4.3.2. Statistics

From left to right, Figure 7 plots $L_{\rm bol}/L_{\rm Edd}$ as a function of $D_n(4000)$, ξ_3, and ξ_4 for both QSO2 and Seyfert 2 galaxies samples. One can see from the left panel that the QSO2s with a younger stellar population and higher $L_{\rm bol}/L_{\rm Edd}$ closely follow the anticorrelation between $L_{\rm bol}/L_{\rm Edd}$ and $D_n(4000)$ that was previously well established in local AGNs (e.g., Kewley et al. 2006; Wang et al. 2011; Mullaney et al. 2013), which suggests a decrease of $L_{\rm bol}/L_{\rm Edd}$ as the circumnuclear stellar population continuously ages. A Spearman's rank-order test yields a correlation coefficient of $r_s=-0.39$ with $P<10^{-7}$ for the QSO2s. The correlation coefficient is enhanced to be $r_s=-0.46$ with $P<10^{-10}$ when the QSO2s and Seyfert 2 galaxies samples are combined.

Could the $L_{\rm bol}/L_{\rm Edd}$–$D_n(4000)$ anticorrelation be understood by an underlying driver due to the mass of the host galaxies (or SMBHs)? For example, Stanley et al. (2017) indicate that the enhanced star formation rate in luminous QSOs results from the fact that luminous QSOs tend to occur in massive galaxies. To test this alternative, we separate the QSO2s into four groups according to their SMBH masses, which are believed to be related to the mass of the bugle of the host galaxies, and show the four groups in panel (a) of Figure 7 using different colors. It is clear that the $L_{\rm bol}/L_{\rm Edd}$–$D_n(4000)$ sequence is still valid for the QSO2s with comparable SMBH masses, although there is a dependence of the sequence on the SMBH masses.

The relationships between $L_{\rm bol}/L_{\rm Edd}$ and the [O III] emission-line profile parameters, ξ_3 and ξ_4, are examined in the middle and right panels of Figure 7, respectively. Again, the corresponding Spearman's rank-order test results are listed in Table 2. Thanks to their high luminosity, the inclusion of the QSO2s therefore reinforces our previous claim that high $L_{\rm bol}/L_{\rm Edd}$ is necessary for both strong blue asymmetry and a strong broad component of the [O III] emission line. In fact, Zhang (2021) recently analyzed the properties of the line wing of the [O III] emission line of 535 type I quasars by using SDSS optical spectral data and pointed out a dependence of the line wing on the $L_{\rm bol}/L_{\rm Edd}$.

As in Wang et al. (2011), a correlation between $L_{\rm bol}/L_{\rm Edd}$ and Δv is found neither in the QSO2s sample nor in a merged sample containing both QSO2s and Seyfert 2 galaxies.

5. Discussion

5.1. The Young Stellar Population Associated with the QSO2s

We argue that it is difficult for the young stellar populations identified in the QSO2s by the Lick $D_n(4000)$ index to be explained as contaminations caused by an underlying AGN continuum. On the one hand, a two-order polynomial, which accounts for an AGN's continuum and an intrinsic extinction, has been involved in our modeling of the continuum of the QSO2s in the `pPXF` package. On the other hand, a comparison study in Wang (2015) shows that ignoring the AGN's continuum will cause only a little underestimation of the measured $D_n(4000)$ value. The level of the underestimation has, however, no evident effect on the fact that QSO2s are typically associated with a young stellar population.

The fact that the QSO2s are associated with a younger stellar population than the Seyfert galaxies, we argue, is not due to the aperture effect caused by the fixed 3″ fiber width adopted by the SDSS. The measured $D_n(4000)$ is plotted as a function of z in Figure 8 for a comparison between the QSO2s and the

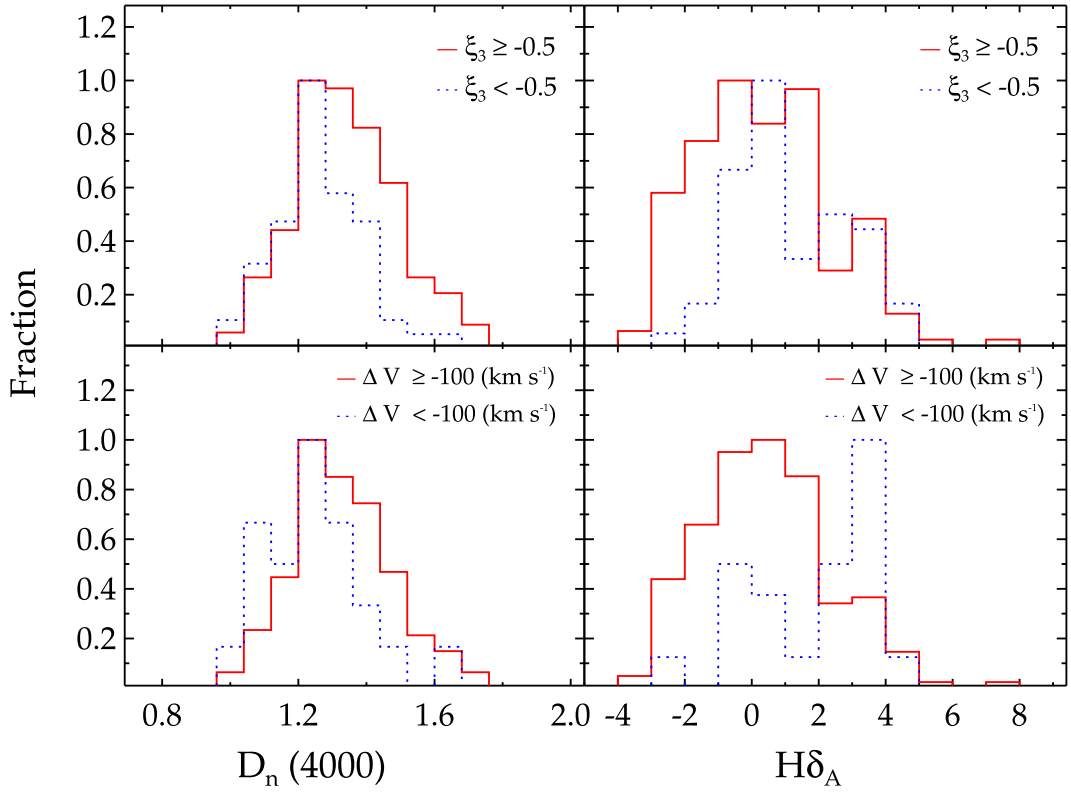

Figure 6. A comparison of the distribution of $D_n(4000)$ (the left column) and $H\delta_A$ (the right column) between the two groups of QSO2s with different shape parameters, ξ_3, and bulk velocity shifts of the [O III] line.

Table 3
Matrix of the Two-sided K-S Tests

Property	$D_n(4000)$ (1)	$H\delta_A$ (2)
ξ_3	$0.32(2 \times 10^{-4})$	$0.25(7 \times 10^{-3})$
Δv	$0.29(6 \times 10^{-2})$	$0.45(4 \times 10^{-4})$

Seyfert 2 galaxies. At first, the QSO2s and Seyfert galaxies overlap with each other within a redshift range from 0.05 to 0.15. In this common redshift range, the median values of $D_n(4000)$ within each redshift bin of 0.05 reinforce the conclusion that QSO2s are generally associated more with younger stellar populations than Seyfert galaxies are. Second, the stellar population age of the bulge of the high-redshift QSO2s is expected to likely be overestimated due to the fixed aperture size because of the radial color gradient of galaxies, which partially results from stellar population age (e.g., Liao & Cooper 2023; and references therein).

Finally, although not as strong as in the Seyfert galaxies, the value of $D_n(4000)$ slightly decreases with redshift for the QSO2s, which is likely due to a cosmic evolution effect. It seems that the slight decrease of $D_n(4000)$ with redshift could not be solely explained by a selection effect on luminosity, in which high-z QSO2s tend to be more luminous and be associated with younger stellar populations. The comparisons in Figure 2, in fact, show that the distributions of [O III] line luminosity have no clear difference between the 221 QSO2s and the parent sample in both redshift bins.

The young stellar populations in QSO2s have been frequently claimed in previous studies, which implies a quasi-simultaneously triggered central AGN activity and circumnuclear starburst (e.g., Heckman et al. 1997; Canalizo & Stockton 2000, 2001; Brotherton et al. 2002; Holt et al. 2007; Wills et al. 2008; Liu et al. 2009; Tadhunter et al. 2011; Villar-Martín et al. 2012; Bessiere et al. 2014, 2017). For instance, by fitting the spectra of 21 QSO2s through the galaxy stellar populations analysis method, Bessiere et al. (2017) show that 71% of the QSO2s in the sample contain young stellar populations with an age less than the maximum lifetime of 100 Myr (see also in Bessiere et al. 2014) expected for an AGN (Martini & Weinberg 2001). By identification of the UV absorption features such as Si IIIλ1417 caused by late O and early B supergiants, a young stellar population with an age of $\sim$6 Myr has been revealed in the nearby QSO2s Mrk 447 (Heckman et al. 1997). In addition, young stellar populations with $t < 0.1$ Gyr are frequently or dominantly found in the quasar-like luminous objects with $L_{[OIII]} > 10^{42}$ erg s^{-1} (e.g., Canalizo & Stockton 2000; Holt et al. 2007; Wills et al. 2008; Tadhunter et al. 2011).

5.2. L_{bol}/L_{Edd}-driven Feedback

Our study shows that the outflow from central SMBHs in QSO2s, as traced by the [O III] line profiles (i.e., ξ_3 and ξ_4), generally increases with the L_{bol}/L_{Edd} (see panels (b) and (c) in Figure 7), which suggests a L_{bol}/L_{Edd}-driven feedback and is consistent with not only the observational studies in the past decade but also the model predictions.

On the observational ground, there were plentiful studies focusing on the relation between the outflow kinematics and the accretion activity of central SMBHs in the past decade for not only Seyfert galaxies but also their luminous cousin, quasars. Briefly speaking, the outflow strength is found to increase, with SMBH's accretion activity assessed in multiple

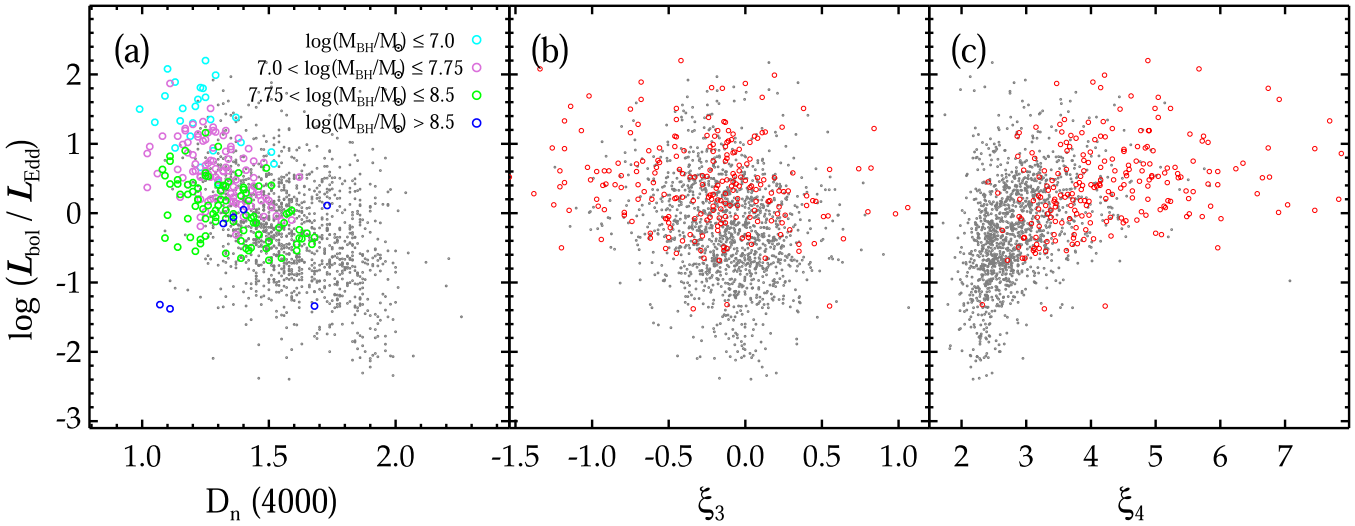

Figure 7. The relationships between $L_{\rm bol}/L_{\rm Edd}$ and $D_n(4000)$ (left panel), and the line profile parameters of ξ_3 (middle panel), and of ξ_4 (right panel). The symbols again are the same as in Figure 4.

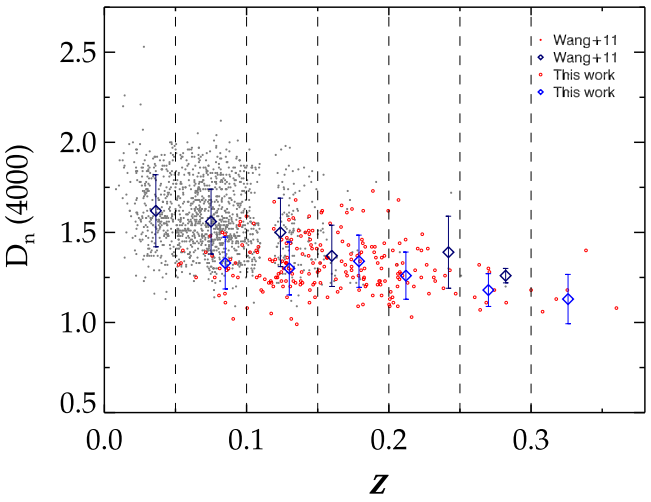

Figure 8. $D_n(4000)$ plotted against redshift for the QSO2s (the red open circles) and Seyfert galaxies (the gray dots). The median values of $D_n(4000)$ determined in each redshift bin of 0.05 are marked by the black and blue diamonds for the QSO2s and Seyfert galaxies, respectively.

ways, including bolometric luminosity $L_{\rm bol}$, [O III]λ5007 line luminosity, intrinsic hard X-ray luminosity, $L_{\rm bol}/L_{\rm Edd}$, and radio power (e.g., Greene & Ho 2005; Mullaney et al. 2013; Bae & Woo 2014; Harrison et al. 2014; Zakamska & Greene 2014; Wang et al. 2016, 2018; Woo et al. 2016; Kong & Ho 2018; Davies et al. 2020). In addition, as shown in Figure 7, the QSO2s show stronger feedback than the Seyfert galaxies due to their higher $L_{\rm bol}/L_{\rm Edd}$.

On the theoretical ground, the observed outflow is believed to result from the wind/radiation pressure launched from the inner accretion disk in the wind/radiation model (e.g., Murray & Chiang 1995; Proga et al. 2000; Crenshaw et al. 2003; King & Pounds 2003; Pounds et al. 2003; King 2005; Ganguly et al. 2007; Reeves et al. 2009; Alexander et al. 2010; Dunn et al. 2010; King et al. 2011; Fabian 2012; Zubovas & King 2012), which successfully explained the fast outflows suggested by the blueshifted ultraviolet and X-ray absorption lines (such as Fe XV and Fe XVI; e.g., Tombesi et al. 2012; Higginbottom et al. 2014). Even though the specific launch mechanism is still under debate, the extension of the wind launched from the accretion disk can reach the inner narrow emission-line region (e.g., Proga et al. 2008), which is supported by recent observations (e.g., Fischer et al. 2018; Kang & Woo 2018; Husemann et al. 2019). In addition, in the merger scenario (e.g., Di Matteo et al. 2005; Springel et al. 2005; Hopkins et al. 2006), strong feedback attributed to AGN activity is required not only to make the quasar activity detectable in optics by removing the material enshrouding the central SMBH (e.g., Hopkins et al. 2005) but also to regulate SMBH growth through quenching the surrounding star formation activity (e.g., Alexander & Hickox 2012; Fabian 2012; Kormendy & Ho 2013).

5.3. Feedback in the Coevolution of AGNs and Their Hosts

Similar to in Seyfert galaxies, we here identify a dependence of ionized gas outflow caused by the SMBH's accretion on the circumnuclear stellar population in QSO2s: a young stellar population (and also high $L_{\rm bol}/L_{\rm Edd}$) is related to a strong outflow. This result follows the coevolutionary scenario proposed previously (e.g., Wang 2015) in which AGNs likely evolve from a high-$L_{\rm bol}/L_{\rm Edd}$ state with strong outflow to a low-$L_{\rm bol}/L_{\rm Edd}$ state with weak outflow as the newly formed circumnuclear massive stars fade out continually. Recent integral field spectroscopic observations of AGNs in fact reveal that the stronger the outflows, the higher the star formation rate (SFR) and the higher the H I gas fraction will be (e.g., Figures 6 and 9 in Woo et al. 2020; Luo et al. 2021, and references therein).

The revealed dependence of outflow on the stellar population implies an evolution of the feedback of AGNs with their host galaxies. However, whether the feedback effect is caused by the outflow is still under hot debate. In the evolution scenario proposed in Sanders et al. (1988), a quasar is produced by expelling the surrounding gas and dust with a wind from the central SMBH after a merger of two gas-rich galaxies. Such feedback from the powerful AGN wind is actually involved in the early numerical and semianalytical galaxy evolution models to reproduce the $M_{\rm BH}$–$\sigma_\star$ relation and luminosity functions of AGNs by quenching the star formation and blowing the gas or dust away, especially in the young AGN phase (e.g., Fabian 1999; Di Matteo et al. 2005; Hopkins et al.

2005, 2008a; Hopkins et al. 2008b; Springel et al. 2005; Croton et al. 2006; Khalatyan et al. 2008; Somerville et al. 2008; Kauffmann & Heckman 2009).

Recent observations, however, indicate that the AGN's feedback has positive, negative, and even no effect on the evolution of the host galaxies of Seyfert galaxies and quasars (e.g., Almeida et al. 2022; Smirnova-Pinchukova et al. 2022, and references therein). By comparing the specific SFR of AGNs with and without outflows, Woo et al. (2020) proposed a delayed effect of feedback on host galaxies, due to the dynamical time required for outflows to travel the large galaxy disks. The Multi Unit Spectroscopic Explorer integral field spectroscopic observation of nine nearby Palomar–Green quasars shows that the fraction of kinetic power of outflow is $\dot{E}_{\rm kin}/L_{\rm bol} \lesssim 10^{-3}$ (and see also in Fiore et al. 2017; Baron & Netzer 2019; Rojas et al. 2020; Molina et al. 2022), which is much lower than the theoretical requirement of $\dot{E}_{\rm kin}/L_{\rm bol} \approx 0.05$–$0.5$ (e.g., Di Matteo et al. 2005; Springel et al. 2005; Hopkins & Quataert 2010; Zubovas & King 2012).

6. Summary

The evolutionary role of the outflow from QSO2s is examined on a large sample of 221 QSO2s extracted from the QSO2s catalog provided in Reyes et al. (2008). Given our spectral analysis on both the AGN and its host galaxy, the main results are listed as follows:

1. Using the Lick indices as indicators, QSO2s are confirmed to be, on average, associated with younger stellar populations than Seyfert galaxies.
2. Even though in occupation at the high $L_{\rm bol}/L_{\rm Edd}$ end, the QSO2s follow the $L_{\rm bol}/L_{\rm Edd}$-$D_n(4000)$ sequence established from the local, less-luminous Seyfert galaxies, which suggests a coevolution between the accretion activity of the SMBH and the host galaxy.
3. QSO2s with a stronger outflow and higher activity ($L_{\rm bol}/L_{\rm Edd}$) tend to be associated with a younger stellar population, which implies a coevolution between the feedback from the SMBH and the host in QSO2s driven by $L_{\rm bol}/L_{\rm Edd}$: AGNs likely evolve from a high $L_{\rm bol}/L_{\rm Edd}$ state with strong feedback to a low $L_{\rm bol}/L_{\rm Edd}$ state with weak feedback as the circumnuclear stellar population continually ages.

The authors thank the anonymous referee for the careful review and suggestions for improving the manuscript significantly. This work was supported by the National SKA Program of China (grant No. 2022SKA0120103), the Astronomical Union Foundation under grant No. U1831126 and the Natural Science Foundation of Hebei Province No. A2019205100, and by the National Natural Science Foundation of China (grant Nos. 12173009, 12273706 and 12273054). J.W. is supported by the Natural Science Foundation of Guangxi (2020GXNSFDA238018).

Funding for the SDSS has been provided by the Alfred P. Sloan Foundation, the Participating Institutions, the National Science Foundation, the U.S. Department of Energy, the National Aeronautics and Space Administration, the Japanese Monbukagakusho, the Max Planck Society, and the Higher Education Funding Council for England. The SDSS Web Site is http://www.sdss.org/.

The SDSS is managed by the Astrophysical Research Consortium for the Participating Institutions. The Participating Institutions are the American Museum of Natural History, Astrophysical Institute Potsdam, University of Basel, University of Cambridge, Case Western Reserve University, University of Chicago, Drexel University, Fermilab, the Institute for Advanced Study, the Japan Participation Group, Johns Hopkins University, the Joint Institute for Nuclear Astrophysics, the Kavli Institute for Particle Astrophysics and Cosmology, the Korean Scientist Group, the Chinese Academy of Sciences (LAMOST), Los Alamos National Laboratory, the Max-Planck-Institute for Astronomy (MPIA), the Max-Planck-Institute for Astrophysics (MPA), New Mexico State University, Ohio State University, University of Pittsburgh, University of Portsmouth, Princeton University, the United States Naval Observatory, and the University of Washington.

ORCID iDs

S. Jin https://orcid.org/0000-0002-0926-0998
R. J. Shen https://orcid.org/0000-0003-2254-1206
Y. X. Zhang https://orcid.org/0000-0002-6610-5265

References

Abazajian, K. N., Adelman-McCarthy, J. K., Agüeros, M. A., et al. 2009, ApJS, 182, 543
Alexander, D. M., & Hickox, R. C. 2012, NewAR, 56, 93
Alexander, D. M., Swinbank, A. M., Smail, I., McDermid, R., & Nesvadba, N. P. H. 2010, MNRAS, 402, 2211
Almeida, I., Duarte, R., & Nemmen, R. 2022, MNRAS, 509, 5657
Antonucci, R. 1993, ARA&A, 31, 473
Aoki, K., Kawaguchi, T., & Ohta, K. 2005, ApJ, 618, 601
Bae, H.-J., & Woo, J.-H. 2014, ApJ, 795, 30
Bahcall, J. N., Kirhakos, S., Saxe, D. H., & Schneider, D. P. 1997, ApJ, 479, 642
Balogh, M. L., Morris, S. L., Yee, H. K. C., Carlberg, R. G., & Ellingson, E. 1999, ApJ, 527, 54
Baron, D., & Netzer, H. 2019, MNRAS, 486, 4290
Bessiere, P. S., Tadhunter, C. N., Ramos Almeida, C., & Villar Martín, M. 2014, MNRAS, 438, 1839
Bessiere, P. S., Tadhunter, C. N., Ramos Almeida, C., Villar Martín, M., & Cabrera-Lavers, A. 2017, MNRAS, 466, 3887
Binney, J., & Merrifield, M. 1998, Galactic Astronomy (Princeton, NJ: Princeton Univ. Press)
Boroson, T. 2005, AJ, 130, 381
Brotherton, M. S., Green, R. F., Kriss, G. A., et al. 2002, ApJ, 565, 800
Bruzual, A. G. 1983, ApJ, 273, 105
Canalizo, G., & Stockton, A. 2000, AJ, 120, 1750
Canalizo, G. v., & Stockton, A. 2001, ApJ, 555, 719
Cappellari, M. 2017, MNRAS, 466, 798
Cappellari, M., & Emsellem, E. 2004, PASP, 116, 138
Cardelli, J. A., Clayton, G. C., & Mathis, J. S. 1989, ApJ, 345, 245
Carniani, S., Marconi, A., Maiolino, R., et al. 2016, A&A, 591, A28
Ciotti, L., & Ostriker, J. P. 2007, ApJ, 665, 1038
Crenshaw, D. M., Kraemer, S. B., & George, I. M. 2003, ARA&A, 41, 117
Cresci, G., Mainieri, V., Brusa, M., et al. 2015, ApJ, 799, 82
Cresci, G., & Maiolino, R. 2018, NatAs, 2, 179
Cresci, G., Tozzi, G., Perna, M., et al. 2023, A&A, 672, A128
Croton, D. J., Springel, V., White, S. D. M., et al. 2006, MNRAS, 365, 11
Davies, R., Baron, D., Shimizu, T., et al. 2020, MNRAS, 498, 4150
Di Matteo, P., Bournaud, F., Martig, M., et al. 2008, A&A, 492, 31
Di Matteo, P., Combes, F., Melchior, A. L., & Semelin, B. 2007, A&A, 468, 61
Di Matteo, T., Springel, V., & Hernquist, L. 2005, Natur, 433, 604
Draper, A. R., & Ballantyne, D. R. 2012, AAS Meeting, 219, 154.03
Dunn, J. P., Bautista, M., Arav, N., et al. 2010, ApJ, 709, 611
Fabian, A. C. 1999, MNRAS, 308, L39
Fabian, A. C. 2012, ARA&A, 50, 455
Fiore, F., Feruglio, C., Shankar, F., et al. 2017, A&A, 601, A143
Fischer, T. C., Kraemer, S. B., Schmitt, H. R., et al. 2018, ApJ, 856, 102
Förster Schreiber, N. M., Übler, H., Davies, R. L., et al. 2019, ApJ, 875, 21

Ganguly, R., Brotherton, M. S., Cales, S., et al. 2007, ApJ, 665, 990
Ge, J.-Q., Hu, C., Wang, J.-M., Bai, J.-M., & Zhang, S. 2012, ApJS, 201, 31
Granato, G. L., De Zotti, G., Silva, L., Bressan, A., & Danese, L. 2004, ApJ, 600, 580
Greene, J. E., & Ho, L. C. 2005, ApJ, 627, 721
Haehnelt, M. G., Natarajan, P., & Rees, M. J. 1998, MNRAS, 300, 817
Halpern, J. P., & Steiner, J. E. 1983, ApJL, 269, L37
Hao, L., Strauss, M. A., Tremonti, C. A., et al. 2005, AJ, 129, 1783
Harrison, C. M. 2017, NatAs, 1, 0165
Harrison, C. M., Alexander, D. M., Mullaney, J. R., et al. 2016, MNRAS, 456, 1195
Harrison, C. M., Alexander, D. M., Mullaney, J. R., & Swinbank, A. M. 2014, MNRAS, 441, 3306
Heckman, T. M., González-Delgado, R., Leitherer, C., et al. 1997, ApJ, 482, 114
Heckman, T. M., & Best, P. N. 2014, ARA&A, 52, 589
Heckman, T. M., Kauffmann, G., Brinchmann, J., et al. 2004, ApJ, 613, 109
Heckman, T. M., Miley, G. K., van Breugel, W. J. M., & Butcher, H. R. 1981, ApJ, 247, 403
Higginbottom, N., Proga, D., Knigge, C., et al. 2014, ApJ, 789, 19
Hirschmann, M., De Lucia, G., Wilman, D., et al. 2014, MNRAS, 444, 2938
Holt, J., Tadhunter, C. N., & Morganti, R. 2007, in ASP Conf. Ser. 373, The Central Engine of Active Galactic Nuclei, ed. L. C. Ho & J. W. Wang (San Francisco, CA: ASP), 347
Hopkins, P. F., Cox, T. J., Hernquist, L., et al. 2013, MNRAS, 430, 1901
Hopkins, P. F., Cox, T. J., Kereš, D., & Hernquist, L. 2008a, ApJS, 175, 390
Hopkins, P. F., & Hernquist, L. 2009, ApJ, 694, 599
Hopkins, P. F., Hernquist, L., Cox, T. J., et al. 2005, ApJ, 630, 705
Hopkins, P. F., Hernquist, L., Cox, T. J., et al. 2006, ApJS, 163, 1
Hopkins, P. F., Hernquist, L., Cox, T. J., & Kereš, D. 2008b, ApJS, 175, 356
Hopkins, P. F., & Quataert, E. 2010, MNRAS, 407, 1529
Hou, L. G., Han, J. L., Kong, M. Z., & Wu, X.-B. 2011, ApJ, 732, 72
Husemann, B., Bennert, V. N., Jahnke, K., et al. 2019, ApJ, 879, 75
Ishibashi, W., & Fabian, A. C. 2014, MNRAS, 441, 1474
Ishibashi, W., Fabian, A. C., & Canning, R. E. A. 2013, MNRAS, 431, 2350
Kakkad, D., Mainieri, V., Vietri, G., et al. 2020, A&A, 642, A147
Kang, D., & Woo, J.-H. 2018, ApJ, 864, 124
Karouzos, M., Woo, J.-H., & Bae, H.-J. 2016, ApJ, 833, 171
Kauffmann, G., & Haehnelt, M. 2000, MNRAS, 311, 576
Kauffmann, G., & Heckman, T. M. 2009, MNRAS, 397, 135
Kauffmann, G., Heckman, T. M., White, S. D. M., et al. 2003, MNRAS, 341, 33
Kewley, L. J., Dopita, M. A., Sutherland, R. S., Heisler, C. A., & Trevena, J. 2001, ApJ, 556, 121
Kewley, L. J., Groves, B., Kauffmann, G., & Heckman, T. 2006, MNRAS, 372, 961
Khalatyan, A., Cattaneo, A., Schramm, M., et al. 2008, MNRAS, 387, 13
King, A. 2005, ApJL, 635, L121
King, A. R., & Pounds, K. A. 2003, MNRAS, 345, 657
King, A. R., Zubovas, K., & Power, C. 2011, MNRAS, 415, L6
Kirhakos, S., Bahcall, J. N., Schneider, D. P., & Kristian, J. 1999, ApJ, 520, 67
Komossa, S., Xu, D., Zhou, H., Storchi-Bergmann, T., & Binette, L. 2008, ApJ, 680, 926
Kong, M., & Ho, L. C. 2018, ApJ, 859, 116
Kormendy, J., & Ho, L. C. 2013, ARA&A, 51, 511
Liao, L.-W., & Cooper, A. P. 2023, MNRAS, 518, 3999
Liu, G., Zakamska, N. L., Greene, J. E., Nesvadba, N. P. H., & Liu, X. 2013, MNRAS, 436, 2576
Liu, X., Shen, Y., Strauss, M. A., & Greene, J. E. 2010, ApJ, 708, 427
Liu, X., Zakamska, N. L., Greene, J. E., et al. 2009, ApJ, 702, 1098
Luo, R., Woo, J.-H., Karouzos, M., et al. 2021, ApJ, 908, 221
Markwardt, C. B. 2009, in ASP Conf. Ser. 411, Astronomical Data Analysis Software and Systems XVIII, ed. D. A. Bohlender, D. Durand, & P. Dowler (San Francisco, CA: ASP), 251
Martini, P., & Weinberg, D. H. 2001, ApJ, 547, 12
Marziani, P., Zamanov, R. K., Sulentic, J. W., & Calvani, M. 2003, MNRAS, 345, 1133
Menci, N., Fiore, F., Puccetti, S., & Cavaliere, A. 2008, ApJ, 686, 219
Molina, J., Ho, L. C., Wang, R., et al. 2022, ApJ, 935, 72
Mullaney, J. R., Alexander, D. M., Fine, S., et al. 2013, MNRAS, 433, 622
Murray, N., & Chiang, J. 1995, ApJL, 454, L105
Nelson, C., Plasek, A., Thompson, A., Gelderman, R., & Monroe, T. 2004, in ASP Conf. Ser. 311, AGN Physics with the Sloan Digital Sky Survey, ed. G. T. Richards & P. B. Hall (San Francisco, CA: ASP), 83
Page, M. J., Symeonidis, M., Vieira, J. D., et al. 2012, Natur, 485, 213
Perna, M., Arribas, S., Catalán-Torrecilla, C., et al. 2020, A&A, 643, A139
Pounds, K. A., King, A. R., Page, K. L., & O'Brien, P. T. 2003, MNRAS, 346, 1025
Proga, D., Ostriker, J. P., & Kurosawa, R. 2008, ApJ, 676, 101
Proga, D., Stone, J. M., & Kallman, T. R. 2000, ApJ, 543, 686
Ramos Almeida, C., Piqueras López, J., Villar-Martín, M., & Bessiere, P. S. 2017, MNRAS, 470, 964
Reeves, J. N., Sambruna, R. M., Braito, V., & Eracleous, M. 2009, ApJL, 702, L187
Reyes, R., Zakamska, N. L., Strauss, M. A., et al. 2008, AJ, 136, 2373
Rojas, A. F., Sani, E., Gavignaud, I., et al. 2020, MNRAS, 491, 5867
Sander, S. P., & Friedl, R. R. 1988, GeoRL, 15, 887
Sanders, D. B., Soifer, B. T., Elias, J. H., et al. 1988, ApJ, 325, 74
Schlafly, E. F., & Finkbeiner, D. P. 2011, ApJ, 737, 103
Scholtz, J., Harrison, C. M., Rosario, D. J., et al. 2021, MNRAS, 505, 5469
Shankar, F., Marulli, F., Mathur, S., Bernardi, M., & Bournaud, F. 2012, A&A, 540, A23
Shen, Y., & Ho, L. C. 2014, Natur, 513, 210
Shin, J., Woo, J.-H., Kim, M., & Wang, J. 2021, ApJ, 908, 81
Silk, J., & Rees, M. J. 1998, A&A, 331, L1
Smirnova-Pinchukova, I., Husemann, B., Davis, T. A., et al. 2022, A&A, 659, A125
Somerville, R. S., Hopkins, P. F., Cox, T. J., Robertson, B. E., & Hernquist, L. 2008, MNRAS, 391, 481
Spergel, D. N., Verde, L., Peiris, H. V., et al. 2003, ApJS, 148, 175
Springel, V., Di Matteo, T., & Hernquist, L. 2005, MNRAS, 361, 776
Stanley, F., Alexander, D. M., Harrison, C. M., et al. 2017, MNRAS, 472, 2221
Tadhunter, C., Holt, J., González Delgado, R., et al. 2011, MNRAS, 412, 960
Tombesi, F., Cappi, M., Sambruna, R. M., et al. 2012, in ASP Conf. Ser. 460, AGN Winds in Charleston, ed. G. Chartas, F. Hamann, & K. M. Leighly (San Francisco, CA: ASP), 8
Tremaine, S., Gebhardt, K., Bender, R., et al. 2002, ApJ, 574, 740
Valdes, F., Gupta, R., Rose, J. A., Singh, H. P., & Bell, D. J. 2004, ApJS, 152, 251
Veilleux, S., & Rupke, D. S. 2005, in ASP Conf. Ser. 331, Extra-Planar Gas, ed. R. Braun (San Francisco, CA: ASP), 313
Véron-Cetty, M. P., Véron, P., & Gonçalves, A. C. 2001, A&A, 372, 730
Villar Martín, M., Emonts, B., Humphrey, A., Cabrera Lavers, A., & Binette, L. 2014, MNRAS, 440, 3202
Villar, V. A., Berger, E., Chornock, R., et al. 2016, ApJ, 830, 11
Villar-Martín, M., Cabrera Lavers, A., Bessiere, P., et al. 2012, MNRAS, 423, 80
Villar-Martín, M., Humphrey, A., Delgado, R. G., Colina, L., & Arribas, S. 2011, MNRAS, 418, 2032
Wang, J. 2015, NewA, 37, 15
Wang, J., Mao, Y. F., & Wei, J. Y. 2011, ApJ, 741, 50
Wang, J., Xu, D. W., Wang, Y., et al. 2019, ApJ, 887, 15
Wang, J., Xu, D. W., & Wei, J. Y. 2016, AJ, 151, 81
Wang, J., Xu, D. W., & Wei, J. Y. 2018, ApJ, 852, 26
Wills, K. A., Tadhunter, C., Holt, J., et al. 2008, MNRAS, 385, 136
Woo, J.-H., Bae, H.-J., Son, D., & Karouzos, M. 2016, ApJ, 817, 108
Woo, J.-H., Son, D., & Bae, H.-J. 2017, ApJ, 839, 120
Woo, J.-H., Son, D., & Rakshit, S. 2020, ApJ, 901, 66
Worthey, G., & Ottaviani, D. L. 1997, ApJS, 111, 377
Xu, D., & Komossa, S. 2009, ApJL, 705, L20
York, D. G., Adelman, J., Anderson, J. E. J., et al. 2000, AJ, 120, 1579
Yuan, S., Strauss, M. A., & Zakamska, N. L. 2016, MNRAS, 462, 1603
Zakamska, N. L., & Greene, J. E. 2014, MNRAS, 442, 784
Zakamska, N. L., Strauss, M. A., Krolik, J. H., et al. 2003, AJ, 126, 2125
Zamanov, R., Marziani, P., Sulentic, J. W., et al. 2002, ApJL, 576, L9
Zhang, K., Wang, T.-G., Yan, L., & Dong, X.-B. 2013, ApJ, 768, 22
Zhang, X. 2021, ApJ, 909, 16
Zubovas, K., & King, A. R. 2012, in ASP Conf. Ser. 460, AGN Winds in Charleston, ed. G. Chartas, F. Hamann, & K. M. Leighly (San Francisco, CA: ASP), 235
Zubovas, K., Nayakshin, S., King, A., & Wilkinson, M. 2013, MNRAS, 433, 3079